

We are IntechOpen, the world's leading publisher of Open Access books Built by scientists, for scientists

6,900

Open access books available

186,000

International authors and editors

200M

Downloads

Our authors are among the

154

Countries delivered to

TOP 1%

most cited scientists

12.2%

Contributors from top 500 universities



WEB OF SCIENCE™

Selection of our books indexed in the Book Citation Index
in Web of Science™ Core Collection (BKCI)

Interested in publishing with us?
Contact book.department@intechopen.com

Numbers displayed above are based on latest data collected.
For more information visit www.intechopen.com



Study on Specific Coefficient in Micromachining Process

Sung-Hua Wu

Abstract

The study proposed an important micro-specific coefficient based on the mathematical modeling of micro-cutting resistance to predict the mechanic conditions at cutter-edge radius. For the steady-state chip formation in the micro-cutting process, the differential angle is usually constant, and the plowing angle and rake angle are relative to the tool-edge radius, cutting resultant force, plowing resistance, surface roughness, and shearing resistance on the tool-workpiece. The optimal process included a cut of depth of 0.001 mm, cutting length of 0.003 mm, cutter-edge temperature of 38°C, and an edge radius of 0.0005 mm on workpiece Al-7075; the optimal cutting force in x-axis was 0.0005 N (Avg.) and the optimal cutting force in y-axis was 0.00028 N (Avg.) for better surface roughness $R_a = 0.16$. The higher temperature was 42.16°C on the workpiece and tool HSS, and the maximum strain rate occurred on the chip shearing zone was 9.33E6 (/s), which obeyed the generalized cutting criterion by numerical analysis. While the micro-specific coefficient is close to 1, the plowing zone will increase friction, stress, resistance, and even cutting excited vibration, resulting in discontinuous chipping. Besides, the process developed the micro-MDOF cutting dynamics model and applied a fractal equation to simulate the micro-cutting process. The validation can be proved as the derived theory agreed well with the simulation in the micro-cutting process.

Keywords: specific coefficient, fractal equation, micro-cutting, steady-state chip formation, micro-MDOF cutting dynamics

1. Introduction

Micro-cutting process for depth of cut and feed is so small that it is very hard to observe under a microscope. Due to the size effect of the cutter-edge radius for larger influence on plowing and shearing zones, it results in increased friction heat, cutting force and, furthermore, specific energy. The study proposed the micro-resistance model of plowing and shearing in the quasi-state cutting process by analytic geometry. Using the fractal equation can help us to build the relations of chip fractal geometry and specific energy. The famous scholar Mandelbrot gave the set [1] is a compact set (**Figure 1**), where resisted of complex numbers c , and he studied space of quadratic polynomials and proposed the function $f_c(z)$ existed non-diverged and iterated from z equals zero. The fractal properties have self-similarity, hyperbolic components, and local connectivity from a topological space x . The author observed the properties of self-similarity of fractal existing on undeformed chip geometry through a series of cross-section projections on a

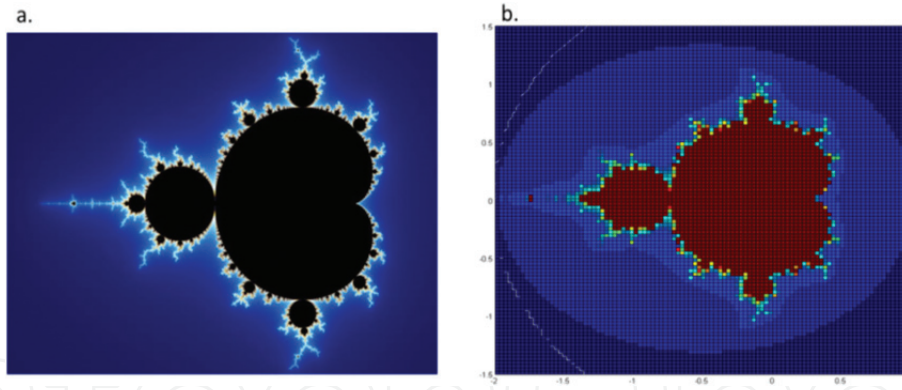


Figure 1.
(a) Mandelbrot set of fractal; and (b) the author's program by complex [5].

sinusoidal wave. The undeformed chip geometry through a series of cross-section projection on a sinusoidal wave by mathematical modeling belongs to a kind of Koch curve transformation, where the Koch curve belongs to a kind of triangle fractal as shown in **Figure 2(d)**. The fractal similarity can be applied in microanalysis of chip formation through enlarging the contour of the chip topograph as shown in **Figure 2(c)**. From another view as shown in **Figure 2(f)**, the fractal geometry is similar to a series of projections of sinusoidal multi-cutter as a rectangle (**Figure 3(d)**). Through analytic geometry, the fractal differential equation can be established to understand chip shapes, chip load, tool geometry, and specific energy. From the view under a microscope, the chip formation is similar (**Figure 2(d)–(f)**) in different views of fractal geometry. Hence, the fractal topograph of **Figure 2** is very important to establish a generalized mathematical model by the analysis of chip fractal geometry. By Fractal mathematical method, the calculation can be achieved less hardware and higher precisely results as **Figure 1(b)**. Due to the excellent calculation and algorithm, material processing or cutting dynamics can

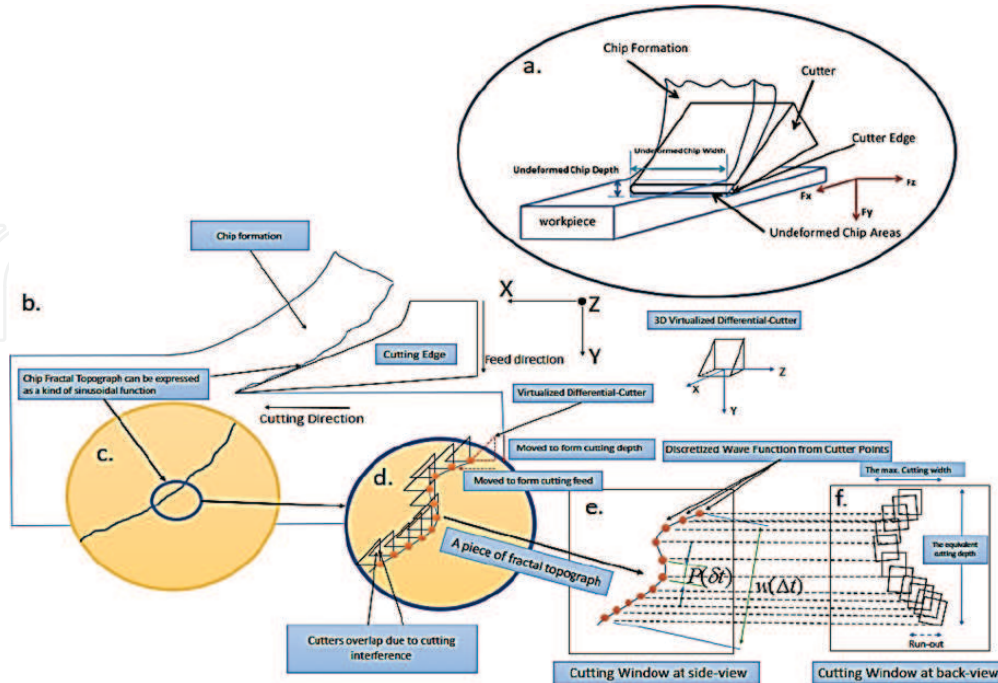


Figure 2.
Undeformed chip areas and deformed chip shapes: (a) the 3-D expression of undeformed cutting areas and chip formation; (b) the side view for chip fractal topograph; (c) to take a part of the contour along the chip edge; (d) the topograph can be simulated by a lot of differential-cutters moved to form cutting depth and feed; (e) the side view of chip topograph can be resisted of cutters under cutting interference in differential time; (f) the state-space transferring for chip fractal topograph into undeformed cutting areas (fractal self-similarity) from (e) to (f).

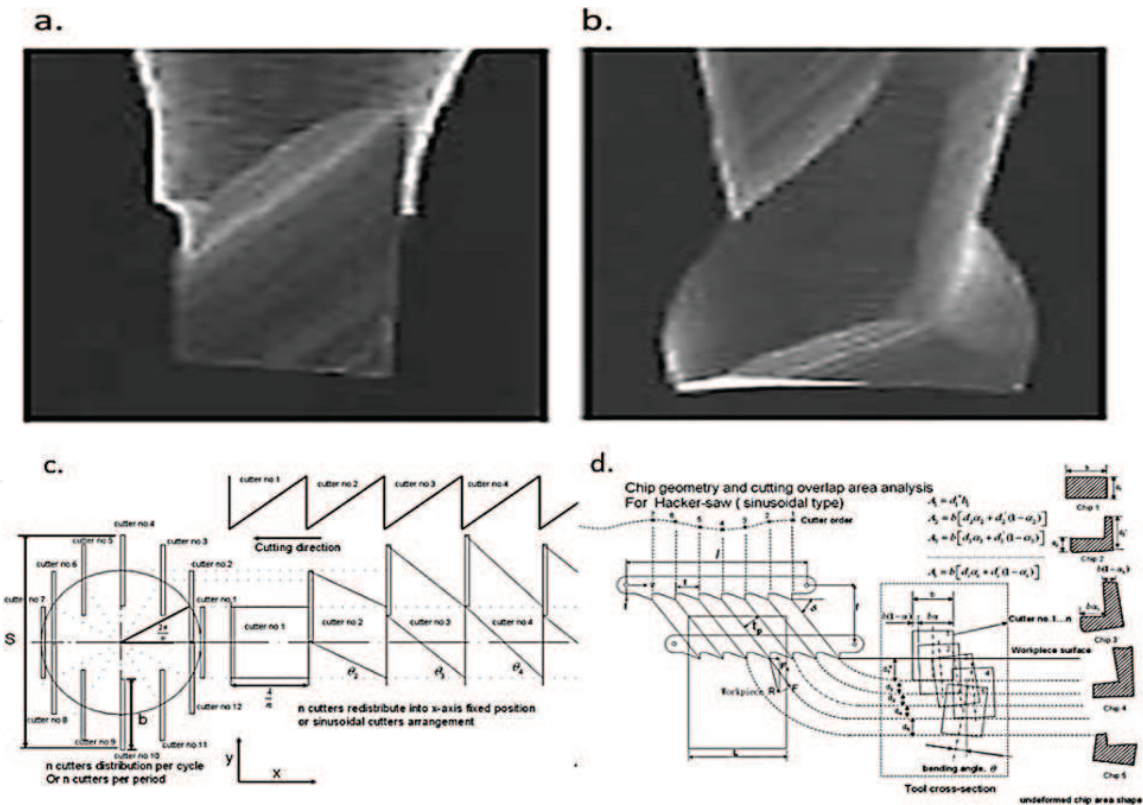


Figure 3.
General micro-cutter: (a) single cutter— $r = 10\text{--}50\text{ }\mu\text{m}$; (b) double cutter—helical angle 30° and $r = 30\text{--}50\text{ }\mu\text{m}$; (c) unit cutters of generalized sinusoidal multi-cutters for the analytic coordinate; and (d) analysis on chip fractal self-similarity of sinusoidal cutter order.

be analyzed by specific energy obtained from undeformed chip formation (Figures 2 and 3). Besides, the theoretical modeling should consider the surface condition of workpiece because the surface roughness and tool size are enlarged in micro-dimension. So, the surface conditions need to be expressed as shown in Figure 4. Hence, the micro-MDOF cutting dynamics model can be developed as Eqs. (22)–(32).

1.1 Paper review

Cao et al. [2] found that the cutting edge radius affects the microscale in the cutting process at a smaller uncut chip thickness by altering the effective rake angle, enhancing the plowing effect and the work affecting the material deformation process, expanding and widening the plastic deformation zone, and causing higher energy dissipation due to increased tool-chip contact length. The author wants to expand the work to develop the theoretical model by advanced mathematics. On the other hand, the study of Cao et al. [2] unestablished the micro-specific coefficient to investigate the relations of factors on plowing, shearing, cutter-edge radius, cutting heat, and stain rate. To extend the study of Cao et al. [2], the fractal equation proposed in Wu [3–5] can be applied on the analysis of variations in chip shapes and undeformed chip formation areas of specific energy obtained. Wu [5] considered the vertical force F_x and horizontal force F_y existing in the mathematical relations as the objective function of the specific energy constant that can achieve the maximum material rate (MMR) through optimization, while a single cutter achieved a steady-state chip formation. The definition of the proportion K_r equals F_y/F_x and the optimal $K_r = 0.602$ for tool HSS and workpiece Al-7075 if the maximum material rate is achieved. The traditional K_r obtained was assumed as the specific energy constant and known cutting force without considering the microscope size effect.

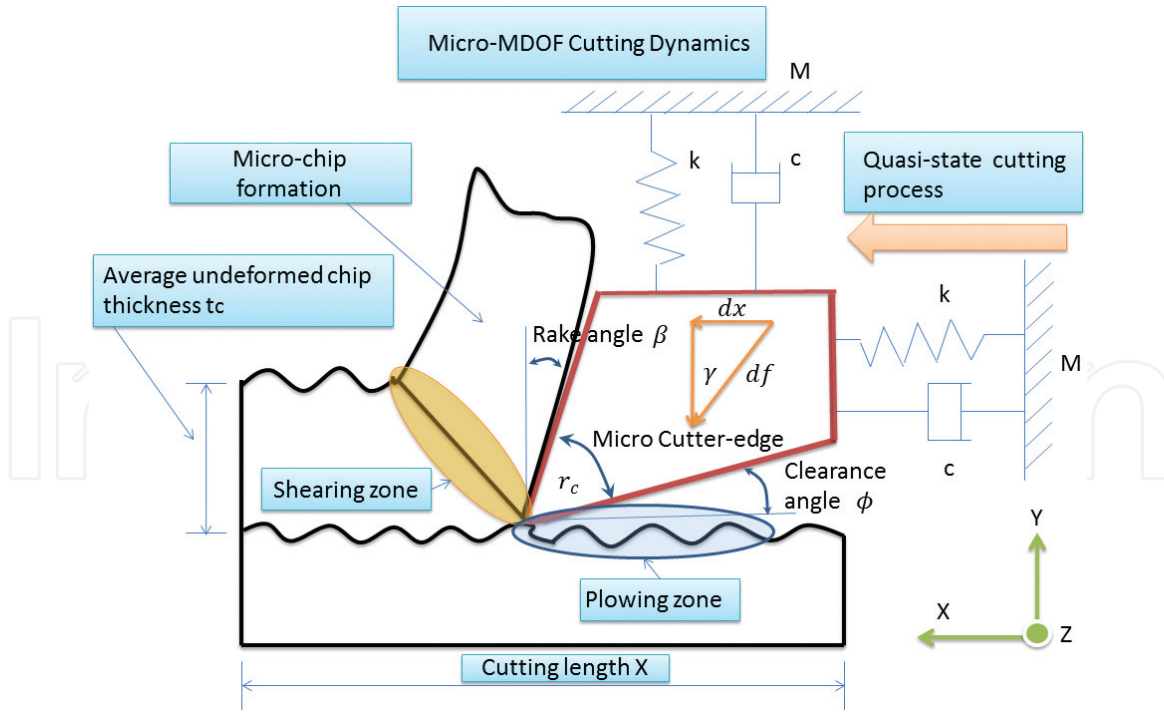


Figure 4.
Micro-MDOF modeling demonstration.

Otherwise, the specific energy and cutting force need to be rebuilt if the material property of workpiece-tool changed. The strategy of micromachining for MMR is also dependent on the optimal specific coefficient obtained by the process, achieving the steady-state chip formation under the known specific energy. Another result expressed a larger excited-vibration while K_r was close to 1 (about 1.1–1.3) through two cutters' simulated design. So, the K_r should be an important factor affecting the cutting stability and MMR in the steady-state cutting process. From the observation of experimental results, a few cutters showed cutter-edge-crack wear similar to the discontinuous wear, and others showed flank wear similar to the continuous wear. The results reminded author Wu that there were some reasons to explain how the shearing and plowing effect occurred on cutter edge in the micromachining process. The study [5] can be extended to investigate the micro-specific coefficient through mathematical derivation. About micromachining, micro-cutting is a general process for the material removal. The key point of micromachining is how to achieve better production precision and reasonable error, even more/less wear on the tool and the maximum material removal rate. David et al. [6] proposed a technique to fabricate the micro-tool, which can achieve a $25\ \mu\text{m}$ diameter and a cutting edge radius curvature of less than $0.1\ \mu\text{m}$ in 6061-T4 aluminum, 4340 steel, and polymethyl methacrylate by focused ion beam. Dib et al. [7] studied minimum chip thickness determination by means of cutting force signal in micromachining. An aluminum alloy (RSA6061-T6) was cut by micro-end mills of carbide. Due to the plowing effect, the material may achieve a height 2–4 times the minimum thickness by using the analysis of cutting force signal of a mini dynamometer. Chae et al. [8] investigated the application by micro-cutting, where a process is expressed to use micro-meso-scale fabrication by miniaturized mechanical material removal processes in creating 3D components using a variety of engineering materials. One of the biggest challenges is to maintain cutting force under a critical limit tool wear and improve productivity. The size effect is also a key question that needs to consider micro-tool geometry, minimum chip thickness, and process parameters. Oliveira et al. [9] studied the relations between size effect and minimum chip thickness in the

micro-milling process. The results showed that the minimum uncut chip thickness varies practically from 1/4 to 1/3 of tool cutting edge. Zhang et al. [10] developed the cutting force in the micro-end-milling process. By considering the theoretical instantaneous uncut chip thickness, the certain critical chip thickness value and minimum uncut chip thickness can be derived by material removal mechanisms. For the micromachining process, tool wear is another key question, where the influence mainly comes from the plowing effect causing larger heat. These two key questions need a good criterion or equation to explain the compliant process. The author Wu expects to find out the key factors for better production quality and establish the equation through the study. Tansel et al. [11, 12] applied a tool wear estimation model to predict the cutting force in micromachining by a neural-network-based method, where the final results achieved to the maximum and minimum errors of 8.84 and 5.09%, respectively. Malekian et al. [13] proposed the minimum uncut chip thickness (MUCT) to study the tool-edge radius in micromachining, resulting in increased machining forces that affect the surface integrity of the workpiece. The results presented that the minimum uncut chip thickness (MUCT) was based on the minimum energy principle and the infinite shear strain and the stagnation point with respect to the edge radius. Wu et al. [14] proposed a groove-sawing model on sinusoidal multi-cutters to investigate the relations between specific energy distribution and the location of tool wear. Hence, the cutters' arrangement, cutters' material, uncut chip shapes, and specific energy can be defined by a fractal equation. Process stability is worthy to understand the development, which can be applied in machining, manufacturing, and design. Afazov et al. [15] found the increase of the cutting forces associated with the variation of the friction conditions between the tool and workpiece contact and stability lobes obtained for different edge radii and rake angles of 0 and 8° in the micro-milling process. The results caused the stability of the process obtained for a wide range of cutter-edge radii, feed rates, and run-out lengths. Filiz et al. [16, 17] have analytically investigated according to a three-dimensional model for micro-end-milling dynamics. The modeling included cross-section and fluted (pre-twisted) geometry and bending and coupled axial/torsional vibrations. Afazov et al. [18, 19] chattered on modeling in micro-milling, where the theory was based on the two degrees of freedom of dynamic parameters for the tool-holder-spindle assembly and the micro-milling cutting forces. Guo et al. [20] applied cutting force modeling for nonuniform helix tools and chip thickness in a five-axis flank milling process by an instantaneous uncut chip thickness (IUCT) model. The final results showed that the difference between helix angles and two edges is small, and the little effect occurred on the cutting forces for the cutting force coefficient prediction error. Malekian et al. [21] established the plowing force model, which can take the effect of elastic recovery based on the interference volume between the tool-workpiece, where the mechanistic model has been verified with experimental cutting force measurements of Al-6061.

2. Theoretical modeling

The process developed the micro-MDOF cutting dynamics model and micro-fractal equation to simulate the micro-cutting process. Through fractal mathematics, the results presented optimal geometric parameters for micro-cutting simulation for tool HSS and workpiece Al-7075 as shown in **Figures 4–6**. The study found that the micro-specific coefficient \hat{K}_t applied in the micromachining process is to explain the influence of shearing and plowing at cutter-edge radius.

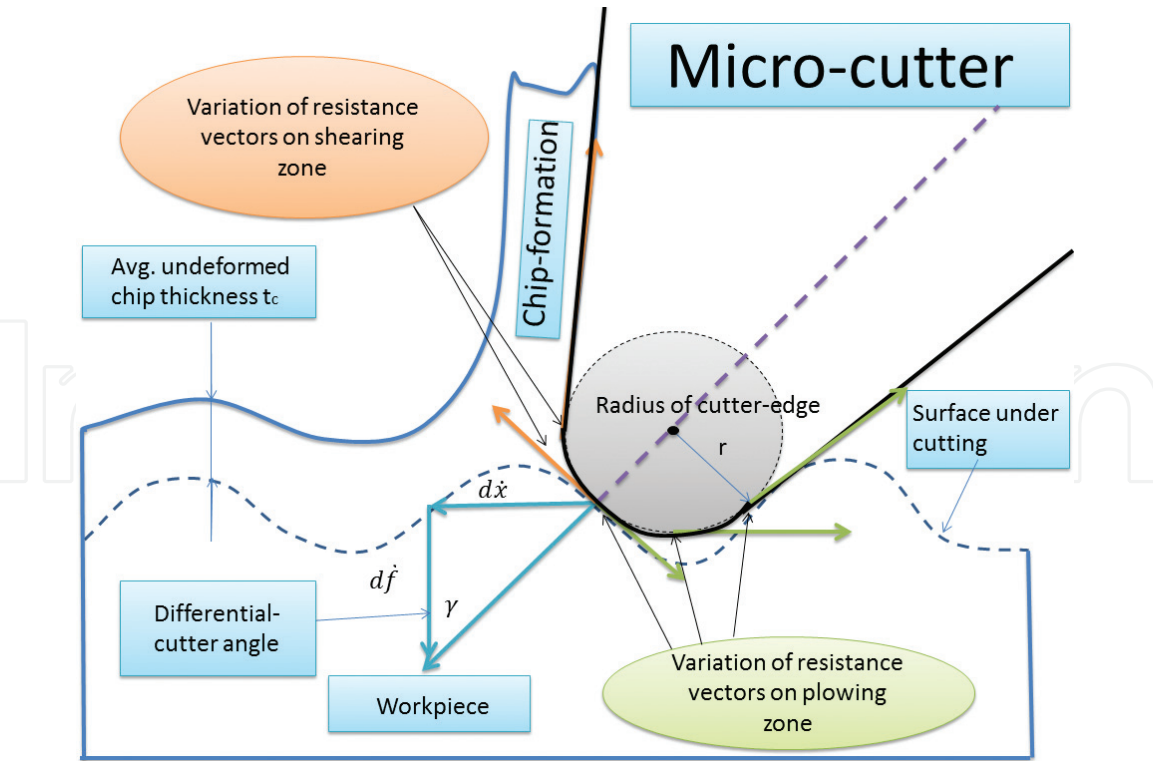


Figure 5.
The relations between micro-cutter-edge radius and chip formation.

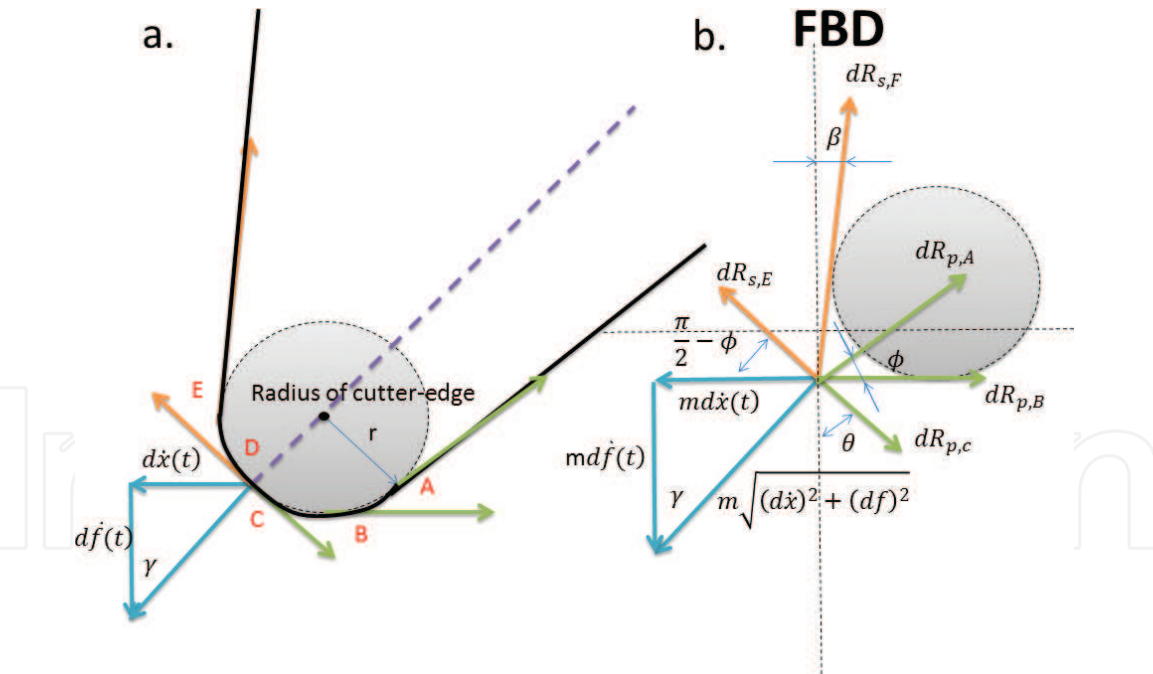


Figure 6.
(a) Vectors of resistance at cutter edge; (b) FBD in the quasi-state micro-cutting process.

2.1 Establishment of the specific coefficient for plowing and shearing resistance in the quasi-state micro-cutting process

The quasi-state micro-cutting process is a dynamical balance process for cutting resistance and cutting force. The three points C, D, and E are aligned as the same points from **Figure 6(a)**. Firstly, the free body diagram (FBD) for plowing and

shearing resistance in the quasi-state micro-cutting process should be established as Eqs. (1) and (2):

$$x \leftarrow + : m\dot{x}(t) + dR_{s,E} \cos\left(\frac{\pi}{2} - \phi\right) - dR_{s,F} \sin(\beta) - dR_{p,A} \cos(\phi) - dR_{p,B} - dR_{p,C} \sin(\theta) = 0 \quad (1)$$

$$y \downarrow + : m\dot{f}(t) - dR_{s,E} \sin\left(\frac{\pi}{2} - \phi\right) - dR_{s,F} \cos(\beta) - dR_{p,A} \sin(\phi) + dR_{p,C} \cos(\theta) = 0 \quad (2)$$

Thus, Eqs. (3) and (4) can be obtained simultaneously as follows:

$$\Rightarrow m\dot{x}(t) + \cos(\phi)[dR_{s,E} - dR_{p,A}] - dR_{s,F} \sin(\beta) - dR_{p,C} \sin(\theta) = dR_{p,B} \quad (3)$$

$$\Rightarrow m\dot{f}(t) - \sin(\phi)[dR_{s,E} + dR_{p,A}] - dR_{s,F} \cos(\beta) + dR_{p,C} \cos(\theta) = 0 \quad (4)$$

For the orthogonal cutting process,

$$\begin{aligned} &\because dR_{s,E} \perp dR_{p,A} \\ &\therefore m\dot{x}(t) - dR_{s,F} \sin(\beta) - dR_{p,C} \sin(\theta) = dR_{p,B} \\ &\Rightarrow m\dot{x}(t) = dR_{s,F} \sin(\beta) + dR_{p,C} \sin(\theta) - dR_{p,B} \end{aligned} \quad (5)$$

Then,

$$m\dot{f}(t) - dR_{s,F} \cos(\beta) + dR_{p,C} \cos(\theta) = 0 \quad (6)$$

Hence,

$$\Rightarrow \tan(\gamma) = \frac{d\dot{x}(t)}{d\dot{f}(t)} = \frac{dR_{s,F} \sin(\beta) + dR_{p,C} \sin(\theta) - dR_{p,B}}{dR_{s,F} \cos(\beta) - dR_{p,C} \cos(\theta)} \quad (7)$$

Due to the size effect with considering the cutter-edge radius r in micromachining process, the differential-cutter angle γ is relative to two factors: plowing angle θ and rake angle β . For the steady-state chip formation in the micro-cutting process, the rake angle β is usually a constant, but the plowing angle θ is relative to the tool-edge precision and surface roughness on the workpiece. For the condition of resistance in the micro-cutting process, cutting resistance on points F, B, and C has a large influence on the steady-state chip formation process. Arc \widehat{FBC} of cutter-edge radius r about $\frac{2\pi}{3}r$ is an important factor, which is needed to consider tool stiffness, geometric design, and material properties in the machining process.

While $\frac{d\dot{x}(t)}{d\dot{f}(t)} = 1$ or close to 1, called plowing and shearing coupling, large plowing resistance $R_{p,B}$ and vibration on the workpiece surface will occur because the plowing zone at B point is very obvious from Eq. (8). The condition should cause an increase in surface roughness:

$$\frac{d\dot{x}(t)}{d\dot{f}(t)} = \hat{K}_r = \frac{dR_{s,F} \sin(\beta) + dR_{p,C} \sin(\theta) - dR_{p,B}}{dR_{s,F} \cos(\beta) - dR_{p,C} \cos(\theta)} = 1 \quad (8)$$

where \hat{K}_r means the specific coefficient of micro-cutting.

Furthermore,

$$\Rightarrow dR_{s,F} \sin(\beta) + dR_{p,C} \sin(\theta) - dR_{p,B} = dR_{s,F} \cos(\beta) - dR_{p,C} \cos(\theta) \quad (9)$$

Going on,

$$\Rightarrow dR_{s,F} [\sin(\beta) - \cos(\beta)] + dR_{p,C} [\sin(\theta) + \cos(\theta)] = dR_{p,B} \quad (10)$$

From integration, we obtain

$$\Rightarrow \int dR_{p,B} = \int [\sin(\beta) - \cos(\beta)] dR_{s,F} + \int [\sin(\theta) + \cos(\theta)] dR_{p,C} \quad (11)$$

To obtain the function of the plowing at B in micromachining process,

$$\Rightarrow R_{p,B} = \int [\sin(\beta) - \cos(\beta)] dR_{s,F} + \int [\sin(\theta) + \cos(\theta)] dR_{p,C} + C \quad (12)$$

Equation (12) is an important result for plowing and shearing influence of micro-cutting under the size effect. While $\frac{d\dot{x}(t)}{d\dot{f}(t)} = \hat{K}_r$ is close to 1, the plowing zone will increase friction, stress, resistance, and even cutting excited-vibration or chipping, resulting in discontinuous chipping. The way to improve is to design the rake angle and cutter-edge radius or raise the tool precision and material.

Although $R_{p,B} = R_{p,B}(R_{s,F}, R_{p,C}, \beta, \theta)$ denoted the resistance function in the micromachining process, the function can be expanded to investigate the relations of factors $R_{p,B}, R_{s,F}, R_{p,C}, \beta, \theta$ combining micro-cutting force, shear stress, strain, and strain rate.

From the view of the micro-cutting process, the definition of micro-specific coefficient is $\hat{K}_r = \frac{d\dot{x}}{d\dot{f}}$, and the definition of average micro-specific coefficient is $\hat{K}_{r, \text{avg}} = \frac{d\dot{x}_2 - d\dot{x}_1}{d\dot{f}_2 - d\dot{f}_1} = \text{slope}$; if $\hat{K}_r = 0$, Eq. (8) can be rewritten as follows:

$$\begin{aligned} dR_{s,F} \sin(\beta) + dR_{p,C} \sin(\theta) - dR_{p,B} &= 0 \\ \Rightarrow dR_{p,B} &= dR_{s,F} \sin(\beta) + dR_{p,C} \sin(\theta) \\ \Rightarrow R_{p,B} &= \int \sin(\beta) dR_{s,F} + \int \sin(\theta) dR_{p,C} + C \end{aligned} \quad (13)$$

The result still expresses that the function $R_{p,B} = R_{p,B}(R_{s,F}, R_{p,C}, \beta, \theta)$ existed.

2.2. Generalized chip load of micro-cutter by the fractal differential equation

According to sinusoidal multi-cutters, the cutters' interference ratio of cutter arrangement can be written as Eq. (14):

$$\alpha_{n+1} = 1 - \frac{\lambda}{nb} (\tan \vartheta_{n+1} - \tan \vartheta_n) \quad (14)$$

where α_{n+1} means $(n+1)^{\text{th}}$ cutter, λ denotes the length of unit wave, n means cutter number of period, b means cutter width, ϑ_{n+1} and ϑ_n means the banding angle of the unit cutter. The equivalent cutting depth of the cutting interference can be presented as Eq. (15):

$$d_{i,eq} = d_1^* \left(\frac{\alpha_i}{1-\alpha_i} \right)^{n-1} + (d_{i-1} - d_{i-2})(1-\alpha_i) + d_1^* \quad (15)$$

where d_1^* means the initial cutting depth and d_i means the transient cutting depth. Considering the cutting depth and cutting width, Eq. (16) can be obtained if the frictional energy dissipated:

$$\begin{aligned} P_i &= A_i = b_i d_i \\ &= (1-\alpha_i) b^* \left[d_1^* \left(\frac{\alpha_i}{1-\alpha_i} \right)^{n-1} + (d_{i-1} - d_{i-2})(1-\alpha_i) + d_1^* \right] \end{aligned} \quad (16)$$

A_i means the undeformed chip shapes, which is also similar to chip fractal geometry areas P_i in the steady-state chip formation process:

$$\begin{aligned} P(d_i, \alpha_i, b, n, \theta_i) \\ = (1-\alpha_i) b^* \left[d_1^* \left(\frac{\alpha_i}{1-\alpha_i} \right)^{n-1} + (1-\alpha_i)(d_{i-1} - d_{i-2}) + d_1^* \right] \end{aligned} \quad (17)$$

Simultaneously,

$$\tan \vartheta = R \sin \left(i \times \frac{2\pi}{n} \right) / t_p \quad (18)$$

where R means amplitude of sinusoidal-set cutters, t_p means cutter pitch, and ϑ denotes the bending angle of sinusoidal multi-cutters.

Equation (19) will delete the overlap ratio $\alpha_i = 0$ if the sinusoidal multi-cutters become a single cutter. On the other hand,

$$\begin{aligned} P &= (1-\phi_i) b^* \left[d_1^* \left(\frac{\phi_i}{1-\phi_i} \right)^{n-1} + (1-\phi_i)(d_{i-1} - d_{i-2}) + d_1^* \right] \\ &= b^* d_1^* \end{aligned} \quad (19)$$

where P means the generalized chip load of the micro-cutter by the fractal differential equation; the average cutting depth d_1^* can be obtained through a few experiments and simulation or specific energy K_t can be obtained if the cutting length b^* is usually constant in the micro-cutting process. Average specific energy K_t can be obtained through unit cutting areas of multi-cutters by average chip load of each chip formation as Eq. (20):

$$\bar{K}_t = \frac{W}{\Delta V} = \frac{P\bar{L}}{b^* d_1^* \bar{L}} = \frac{P}{b^* d_1^*} \quad (20)$$

The cross-sections Type A, Type B, and Type C of undeformed chip shapes can be derived as Eq. (21) and **Figure 7**:

$$\begin{aligned} P_{typeA} &= \bar{K}_t b^* d_1^* \text{ for Type A} \\ P_{typeB} &= \bar{K}_t b^* (1 - \tan \varphi) d_1^* \text{ for Type B} \\ P_{typeC} &= \frac{1}{2} \bar{K}_t b^* d_1^* \text{ for Type C} \end{aligned} \quad (21)$$

2.3 Micro-MDOF cutting dynamics equation

A tiny cutter should have a tiny mass δm , damping c , and elastic constant k with micro-dynamic loading P as shown in **Figure 4**. It needs to construct a dynamic equation as Eq. (22):

$$[\delta m]\{\ddot{x}\} + [c]\{\dot{x}\} + [k]\{x\} = \{p\} \quad (22)$$

Assume the initial condition as

$$\begin{aligned} \{\bar{x}(0)\} &= [\Phi]\{q(0)\} \\ \{\dot{\bar{x}}(0)\} &= [\Phi]\{\dot{q}(0)\} \end{aligned} \quad (23)$$

Substitute $\{x_i\}^T$ into Eq. (22),

$$[\delta m]\{\ddot{x}\} + [c]\{\dot{x}\} + [k]\{x\} = \{p\} \quad (24)$$

Then,

$$\begin{aligned} \{\tilde{x}_i\}^T [\delta m] [\Phi] \{\ddot{q}\} + \{\tilde{x}_i\}^T [c] [\Phi] \{\dot{q}\} + \{\tilde{x}_i\}^T [k] [\Phi] \{q\} &= \{\tilde{x}_i\}^T \{p\} \\ (i = 1, 2, 3, \dots, n) \end{aligned} \quad (25)$$

For orthogonal conditions,

$$\begin{aligned} \{\tilde{x}_j\}^T [\delta m] \{\tilde{x}_i\} &= 0, (i \neq j) \\ \{\tilde{x}_j\}^T [c] \{\tilde{x}_i\} &= 0, (i \neq j) \\ \{\tilde{x}_j\}^T [k] \{\tilde{x}_i\} &= 0, (i \neq j) \end{aligned} \quad (26)$$

Going on,

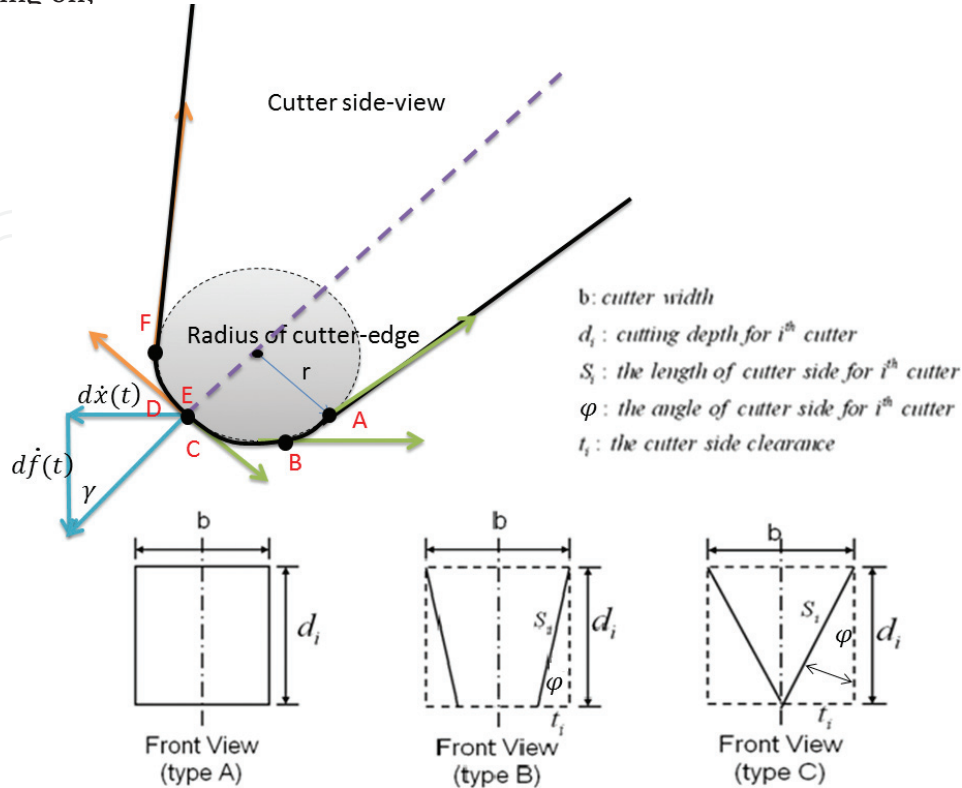


Figure 7.
Variation of cross-section shapes for undeformed chip formation from Type A to Type C.

$$\delta m_i \ddot{q}_i + c_i \dot{q}_i + k_i q_i = p_i, (i = 1, 2, 3, \dots, n) \quad (27)$$

To define

$$\begin{aligned} \delta m_i &= \{\tilde{x}_i\}^T [\delta m] \{\tilde{x}_i\} \\ c_i &= \{\tilde{x}_i\}^T [c] \{\tilde{x}_i\} \\ k_i &= \{\tilde{x}_i\}^T [k] \{\tilde{x}_i\} \\ p_i &= \{\tilde{x}_i\}^T \{p\} \end{aligned} \quad (28)$$

Hence,

$$\ddot{q}_i + \frac{c_i}{\delta m_i} \dot{q}_i + \frac{k_i}{\delta m_i} q_i = \frac{p_i}{\delta m_i} \quad (29)$$

Assume

$$\begin{aligned} \frac{c_i}{\delta m_i} &= 2\xi_i \omega_i \\ \frac{k_i}{\delta m_i} &= \omega_i^2 \end{aligned} \quad (30)$$

Furthermore,

$$\ddot{q}_i + 2\xi_i \omega_i \dot{q}_i + \omega_i^2 q_i = \frac{p_i}{\delta m_i} \quad (31)$$

To solve, the micro-MDOF cutting dynamics equation can be obtained as Eqs. (31) and (32):

$$q_i = q_i(t) = e^{-\xi_i \omega_i t} \left[\frac{\dot{q}_i(0) + \xi_i \omega_i q_i(0)}{\omega_p} \sin(\omega_p t) + q_i(0) \cos(\omega_p t) \right] + \dots \quad (32)$$

($i = 1, 2, 3, \dots, n$)

where $\omega_p = \omega_i \sqrt{1 - \xi_i^2}$.

Equation (32) can be expanded by Taylor series expansion or numerical analysis.

In order to obtain the temperature variation of the cutter edge and chip surface, where the Johnson-Cook equation is used as Eq. (33), the temperature conduction between tool and workpiece is assumed. The study does not consider the cutting temperature conducting into the air:

$$\sigma_{eq} = (A + B \varepsilon_n) \left(1 + C \ln \left(\frac{\dot{\varepsilon}}{\dot{\varepsilon}_0} \right) \right) \left(1 - \left(\frac{T - T_{room}}{T_m - T_{room}} \right)^m \right) \quad (33)$$

where T_m means the melting point temperature, T_{room} means the environmental temperature, T means the workpiece temperature, A means the yielding stress, B means the strain factor, n means the strain coefficient, m means the temperature coefficient, $\dot{\varepsilon}$ means the plastic strain ratio, and ε_0 means the strain ratio. The simulation processed the orthogonal micro-cutting by the Lagrangian finite element method and numerical analysis. Eq. (33) offers the cutting temperature distribution on the tool-workpiece.

3. Results and discussion

The study by micro-MDOF cutting dynamics simulated micro-cutting process according to micro-resistance equations (Eqs. (7) and (12)) at cutter-edge radius in order to validate plowing resistance increasing than shearing, resulted in cutting temperature raising occurred at plowing zone. Simultaneously, the parameter setup of the rake angle at 5, 10, and 15° is presented to observe the relations of plowing zone, heat rate, von Mises stress, cutting force, and specific coefficients. The study did not consider the affection of the tool-HSS elastic deformation, and it needs to focus on the chip formation and shear deformation zone by the size effect. The size effect in micro-cutting process is relative to the theoretical model $R_{p,B} = R_{p,B}(R_{s,F}, R_{p,C}, \beta, \theta)$. The plowing effect at B point is greater than plowing at C and shearing at F if the micro-specific coefficient is close to 1. Hence, another important factor is differential-cutter angle γ relative to undeformed chip thickness if the micro-specific coefficient belongs to a reasonable range to avoid shearing-plowing coupled effect, such as the range $0 \leq \hat{K}_r \leq 0.9$, where $\hat{K}_r = 0$ is similar to the vertical feed on the workpiece or digging process. The variation of differential-cutter angle γ will affect the cutting force because the variation of the resultant force comes from the two component forces $md\dot{x}$ at x-direction and $md\dot{y}$ at y-direction. The resultant force vectors will affect the variation of undeformed chip thickness according to the theoretical model and demonstration in **Figures 4–6**. Therefore, the micro-cutting theory by the size effect is different from the traditional plastic theory. In the micro-cutting process, the tool and workpiece are usually symmetric in the z-direction. In brief, the model can be simplified from three-dimensional to two-dimensional in order to reduce the calculation as shown in **Table 1** and **Figure 8**. The influence of the factor affecting the variation of chip thickness comes from the variation of the resultant force at differential-cutter angle. If the radius of micro-cutter is larger, the resistance at x-direction will become larger due to the contacted areas for arc DE and arc BC increasing at the tool-

Material and tool geometry parameters			
Tool	HSS		
Workpiece	Al-7075		
Length*height (2D)	0.005 mm*0.002 mm		
Cutter-edge radius	0.00005 mm		
Rake angle (°)	5	10	15
Clearance angle (°)	10		
Process parameters			
Feed	0.0005 mm		
Room temp. (°C)	20		
Initial temp. of the workpiece (°C)	20		
Cutting depth (average chip thickness)	0.001 mm		
Cutting condition	Dry cutting		
Cutting velocity (mm/min)	30		
Friction coefficient	0.4–0.5		
Cutter condition	Single-cutter; orthogonal cutting		

Table 1. Simulated parameters.

workpiece interface, and furthermore, the friction and resistance also increase, resulting in the differential-cutter angle varying with increasing resultant force, cutting force increasing with increasing resultant force if the cutting velocity was constant in the x-direction, and finally, the chip thickness varying with variation in the cutting force. From the observation of **Figures 5** and **6**, the resultant force indeed varied with the differential-cutter angle. Hence, the micro-specific coefficient \hat{K}_r varied with the differential-cutter angle, and it was an important factor for the production precision in the machining process.

3.1 Micro-MDOF cutting dynamic simulation

The initial conditions for the material and workpiece as shown in **Table 1** and **Figure 8** can be set up by H-adaptive model fine mesh raising the cutting precision. Von Mises stress can be expressed as the wear on tool flank or the cutting resistance under plastic stress and friction. **Figure 9** demonstrated that the analysis of vectors on cutter-edge radius can prove that plowing at B (934 MPa) is larger than shearing at F (800 MPa) for (c) compared with (b) and (a); (a) theoretical model FBD for micro cutter-edge radius; (b) defined plowing and shearing on cutter radius, where the plowing angle is θ . The shearing and plowing resistance model can be established to predict the influence of tool geometry, rake angle, and plowing angle on the stress of the plowing zone and shearing zone. On the other hand, it can explain why cutting force increased, friction heat increased, and tool flank wear

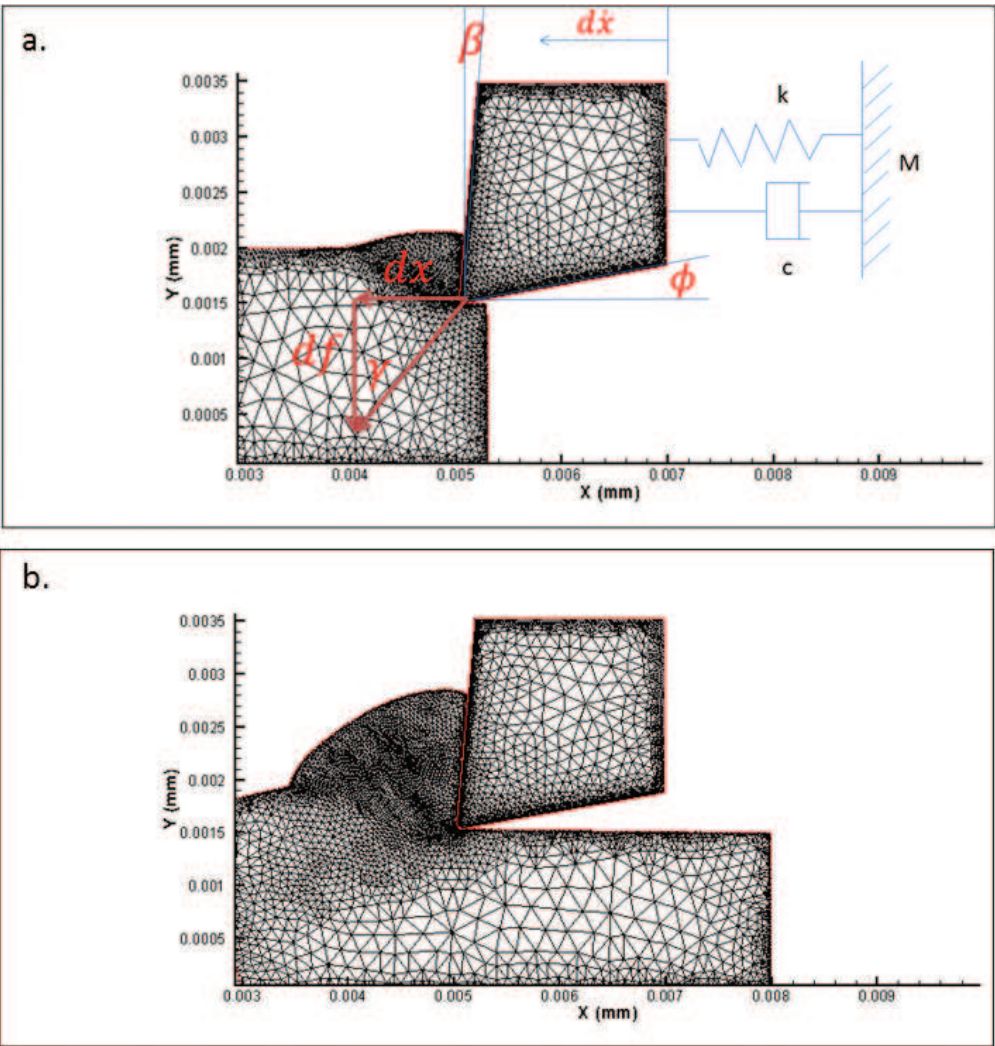


Figure 8.
H-adaptive meshing solid-model; (a) the cut-in process for micro-cutter and (b) the cutting process for steady-state chip formation.

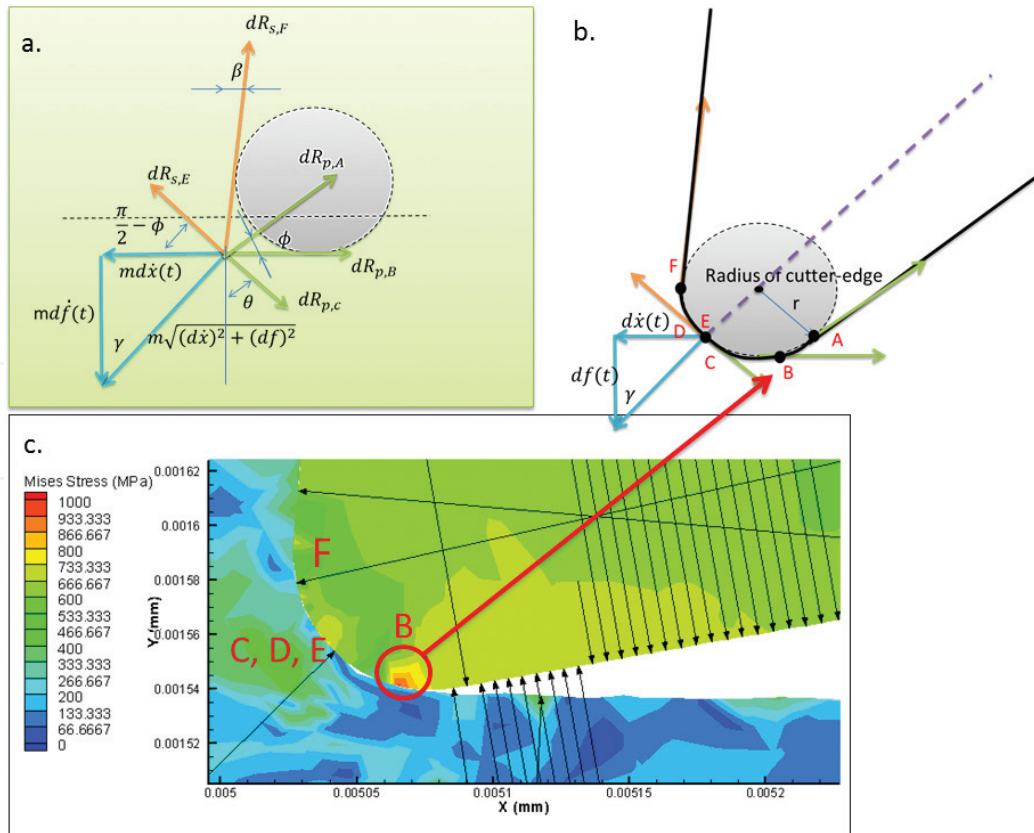


Figure 9.

The analysis of vectors on the cutter-edge radius can prove that plowing at B (934 MPa) is larger than shearing at F (800 MPa) for (c) compared with (b) and (a); (a) theoretical model FBD for micro-cutter-edge radius; (b) defined plowing and shearing on cutter radius; plowing angle is θ .

occurred by the size effect in the micro-cutting process. The finding results offer the importance for micro-MDOF cutting dynamics differed from the traditional cutting process. According to the simulated micro-cutting conditions of cutter-edge radius, the finding results are as follows: the maximum von Mises 934 MPa occurred on tool flank; the maximum heat rate $9.5E^6$ W/mm² occurred on the plowing zone to a part of the shearing zone; the maximum strain rate $9.5E^6$ occurred on the plowing zone to a part of the shearing zone similar to heat rate; and the higher temperature 43.4°C on the whole cutter-edge radius and shearing-plowing zone suffering size effect (Figure 10).

3.2 The relations of rake angle, cutting force, and cutting temperature

The results are nicely reasonable for workpiece Al-7075 and tool HSS. The variation of micro-cutting force is not uniform because of the roughness increasing on the workpiece surface after micro-cutting. The result can be proved by the plowing influence of size effect according to Eq. (7). The optimal process included a cut of depth of 0.001 mm, a cutting length of 0.003 mm, and a cutter edge of 38°C on workpiece Al-7075; the optimal cutting force in x-axis was 0.0005 N (Avg.) and the optimal cutting force in y-axis was 0.00028 N (Avg.) for better surface roughness $R_a = 0.16$. The higher temperature was 42.16°C on workpiece and tool HSS, and the maximum strain rate that occurred on the chip shearing zone was $9.33E06$ (/s). The variation of rake angle compared with cutting force F_x , F_y , and cutting temperature presented that the rake angle 15° has better longer tool life because the cutting force is smaller than others as shown in Figure 11. The results can also be expressed by the resistance at B smaller than others. The cutter with rake angle 15° has lower cutting temperature through a long-time micro-cutting process as Figure 12. The trends of

different rake angles for cutting force and cutting temperature are the same. The trends are nonlinear because of the size effect. The future work can investigate the influence of plowing angle.

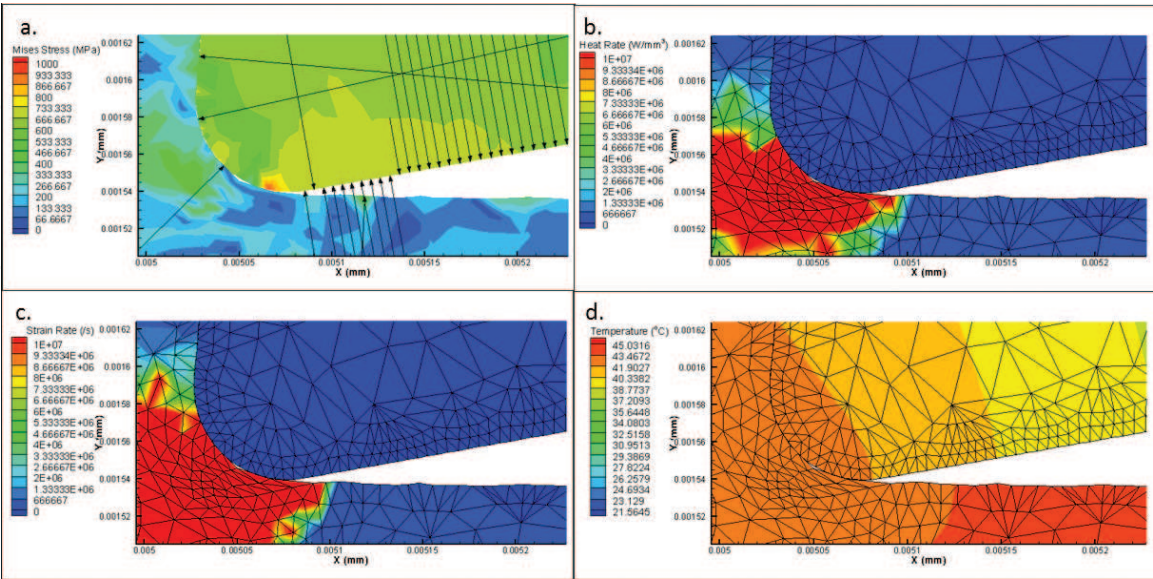


Figure 10.
The simulated micro-cutting conditions of cutter-edge radius. (a) The maximum von Mises 934 MPa occurred on tool flank; (b) the maximum heat rate 9.5×10^6 W/mm² occurred on the plowing zone to a part of the shearing zone; (c) the maximum strain rate 9.5×10^6 occurred on the plowing zone to a part of the shearing zone similar to the heat rate; and (d) the maximum temperature 43.4 °C on the whole cutter-edge radius and shearing-plowing zone suffering from size effect.

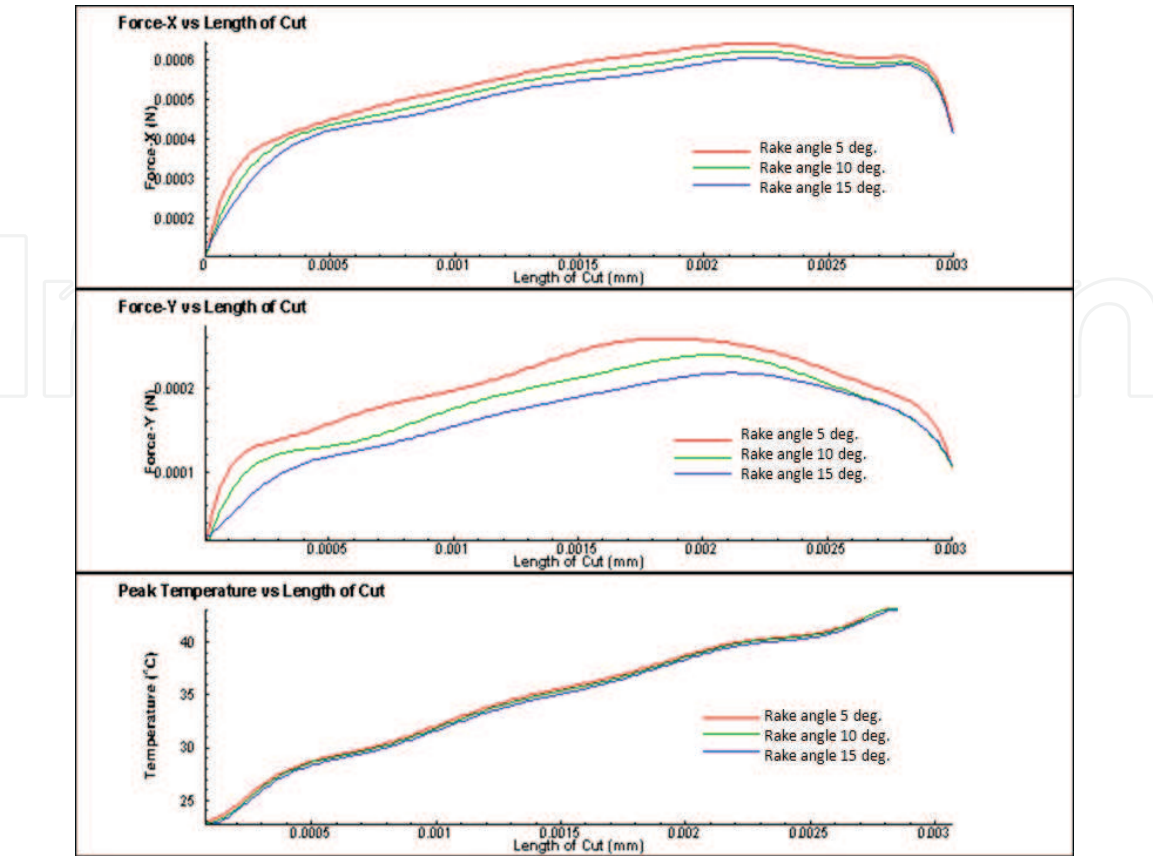


Figure 11.
The variation of rake angle compared with cutting force F_x and F_y and cutting temperature.

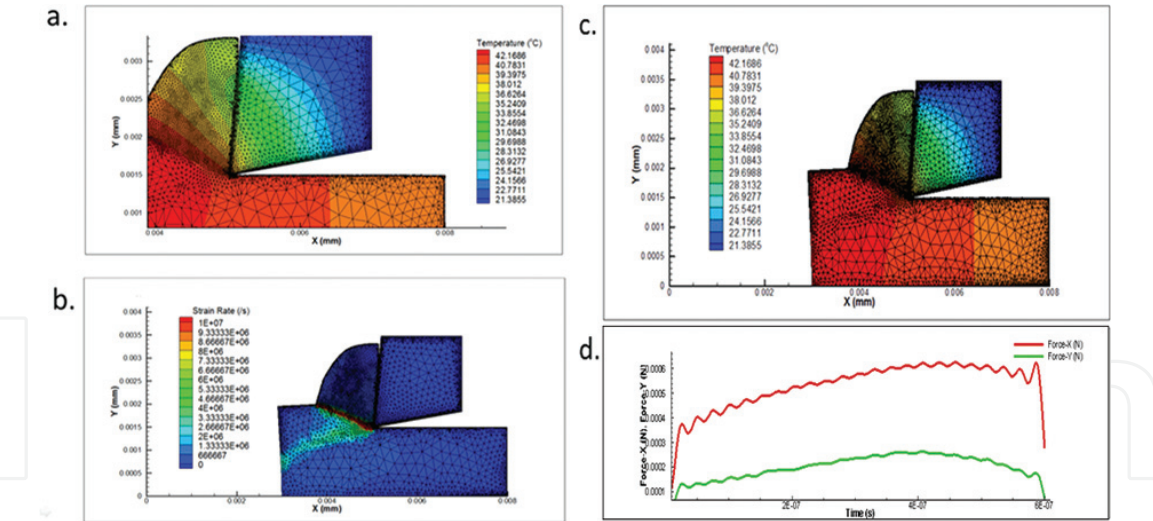


Figure 12. Optimal process parameters in the study included a cut of depth of 0.001 mm, a cutting length of 0.003 mm, and a cutter edge of 38°C on workpiece Al-7075; the optimal cutting force in x-axis was 0.0005 N (Avg.) and the optimal cutting force in y-axis was 0.00028 N (Avg.) for better surface roughness $R_a = 0.16$. The higher temperature was 42.16°C on workpiece and tool HSS, and the maximum strain rate that occurred on the chip shearing plane $\dot{\epsilon}$ was 9.33E06 (/s), which obeyed the generalized cutting criterion by numerical analysis.

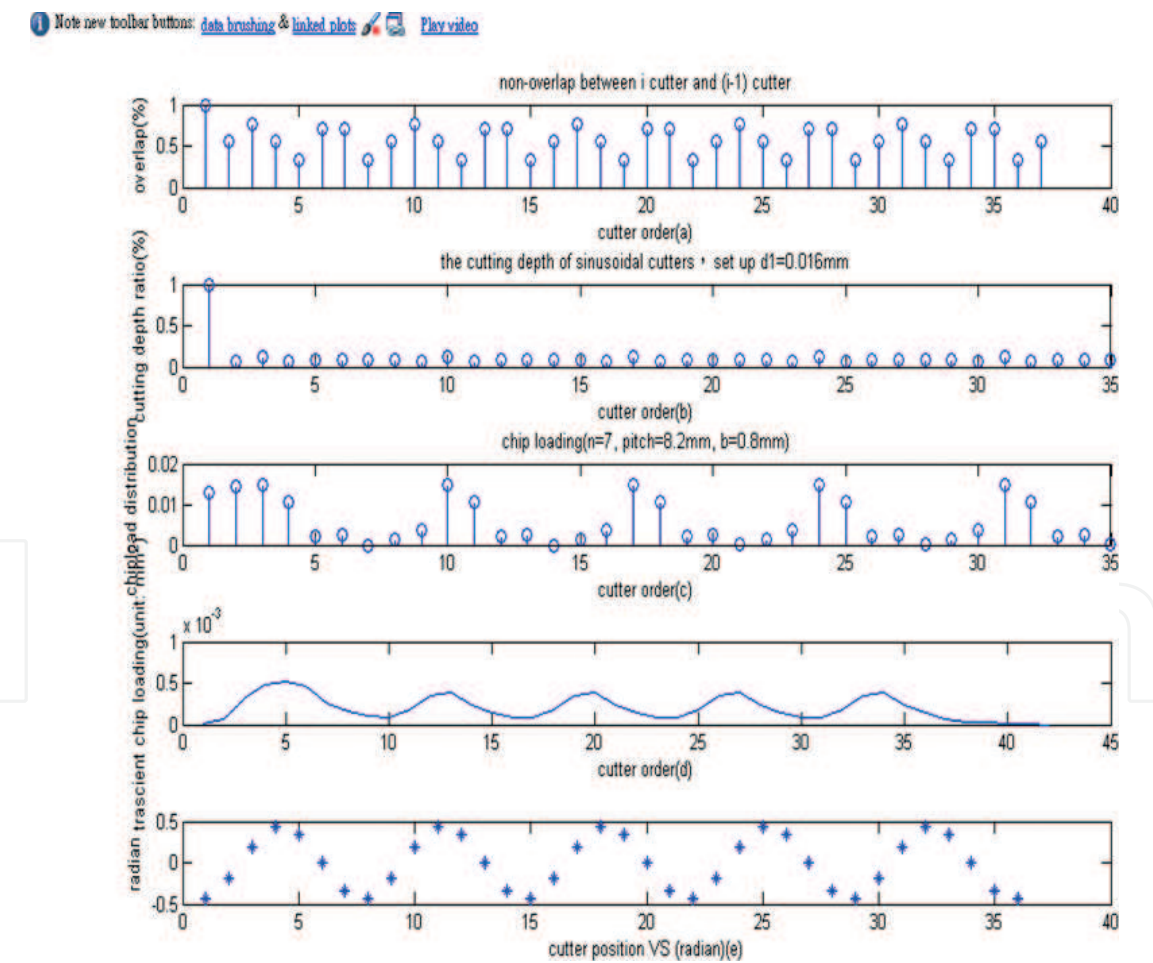


Figure 13. Optimal geometric parameters for micro-cutting simulation for tool HSS and workpiece Al-7075. (a) Non-overlap ratio for sinusoidal multi-cutters, (b) cutting depth ratio for sinusoidal multi-cutters, (c) discrete chip loading distribution, (d) continuous chip loading for multi-cutters, and (e) cutters' arrangement.

3.3 The simulation for multipoints and shearing and plowing

In order to express steady-state continuous chip formation, the cutting of multipoints has been simulated on the quasi-state cutting process as shown in

Figure 13 and the maximum chip loading of $0.56\text{E}^{-3}\text{ mm}^2$ as shown in **Figure 13(d)**. The non-overlap ratio and cutting depth ratio for cutters can be calculated by fractal geometry of the microscope. Through the assumed $d1^* = 0.125\text{ mm}$ of fractal mathematics, the results for multipoint cutting presented optimal geometric parameters for quasi-state cutting simulation of tool HSS and workpiece_Al-7075

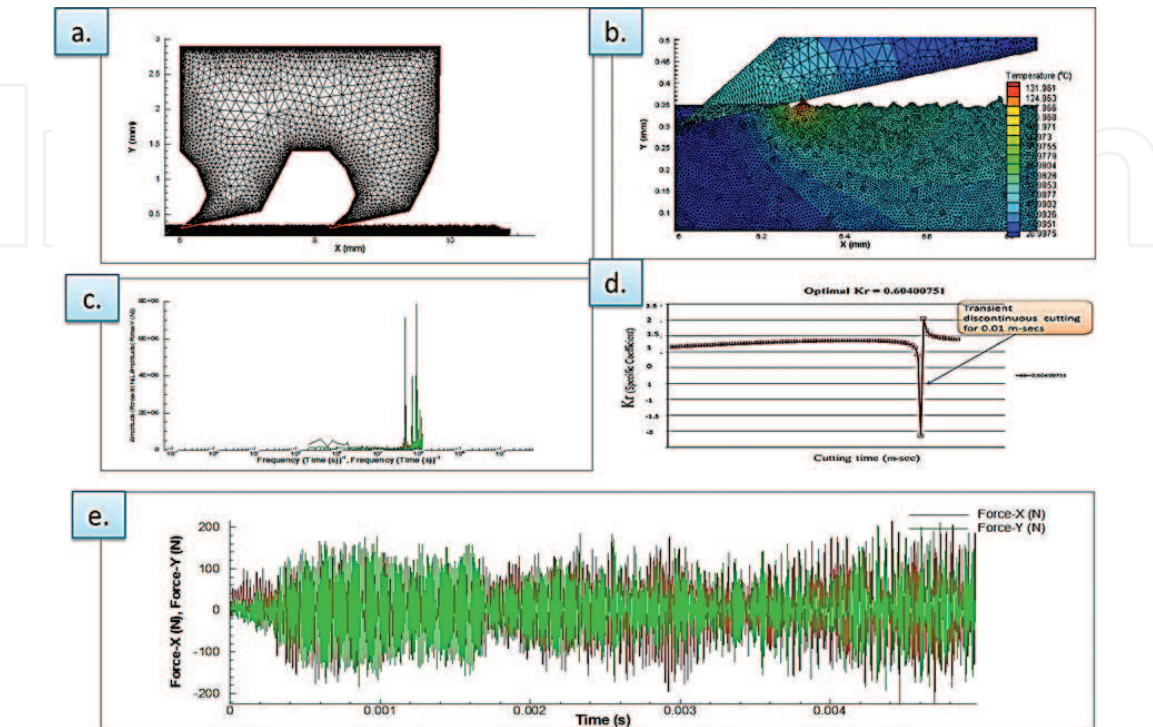


Figure 14. Simulation for two cutters' cutting process [5]: (a) two cutters' modeling; (b) the effects on shearing equals plowing; (c) similar frequency for F_x and F_y ; (d) specific coefficient $K_r = 1.3$ showed discontinuous characteristics; and (e) similar frequency for F_x and F_y and cutting force distribution.

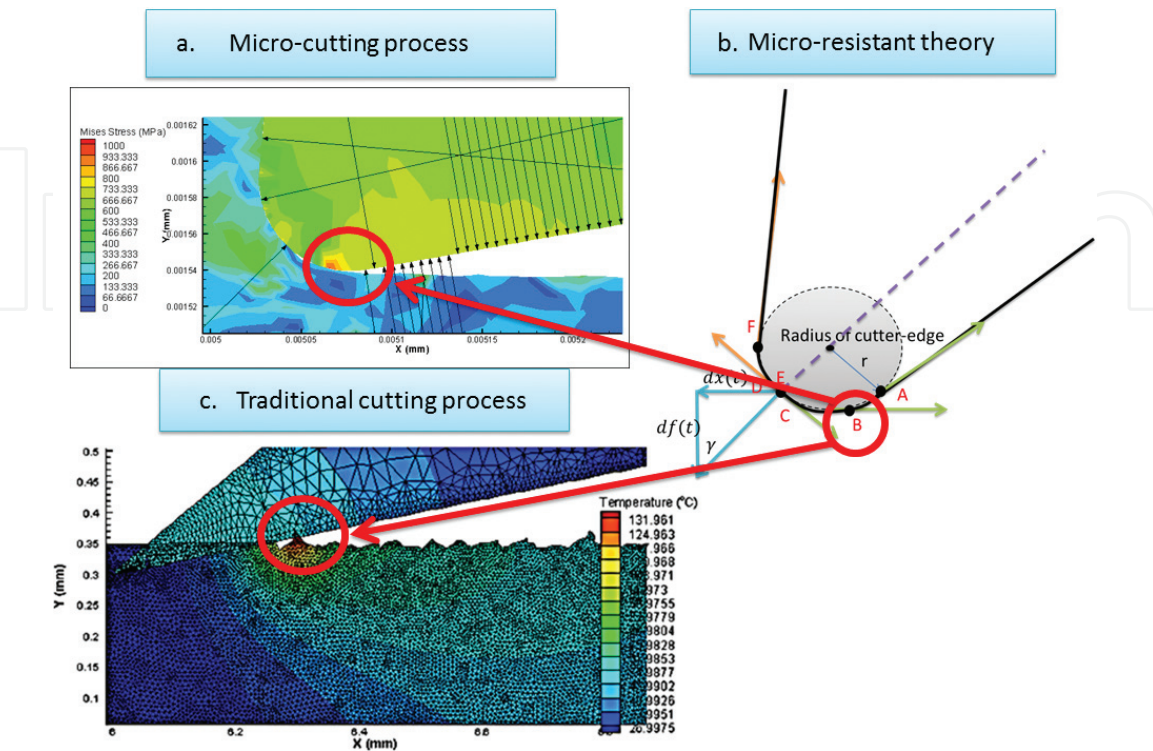


Figure 15. To compare with micro-cutting, the traditional process has the same plowing effect, but the plowing in microscope effect is more obvious. (a) Cutting temperature in micro-cutting process, (b) micro-resistance theory, and (c) cutting temperature in the traditional process.

as shown in **Figure 13**: (a) non-overlap ratio for sinusoidal multi-cutters, (b) cutting depth ratio for sinusoidal multi-cutters, (c) discrete chip loading distribution, (d) continuous chip loading for multi-cutters, and (e) cutters arrangement. **Figure 13(d)** can be expressed as a continuous loading trend for unit period cutting similar to the trend of single cutter in the micromachining process without considering the influence of the size effect. Another simulation is to prove that the plowing and shearing coupling existed while $\frac{d\dot{x}(t)}{df(t)} = \hat{K}_r$ is close to 1 by traditional tool design in the cutting process. The special tool with two cutters of larger cutter-edge radius has simulated K_r to be close to 1 under the traditional cutting as shown in **Figure 14(a)** and **(b)**. The specific coefficient $K_r = 1.3$ showed discontinuous characteristics, where the traditional specific coefficient defined as $K_r = \bar{F}_x / \bar{F}_y$ and \bar{F}_x, \bar{F}_y means the average cutting force. **Figure 14(e)** shows similar frequency for F_x and F_y and cutting force distribution. The excited-vibration of the tool will occur when the micro-specific coefficient \hat{K}_r is close to 1. To compare with micro-cutting, the traditional cutting process has the same plowing effect, but the plowing in microscope effect is more obvious as shown in **Figure 15**. The validation can be proven as the derived theory agreed well with the simulation in the micro-cutting process.

4. Conclusions

The major results have been summarized as follows:

1. The optimal process included a cut of depth of 0.001 mm, a cutting length of 0.003 mm, and a cutter edge of 38°C on workpiece Al-7075; the optimal cutting force in x-axis was 0.0005 N (Avg.) and the optimal cutting force in y-axis was 0.00028 N (Avg.) for better surface roughness $R_a = 0.16$. The higher temperature was 42.16°C on workpiece and tool HSS, and the maximum strain rate that occurred on the chip shearing zone was 9.33E06 (/s), which obeyed the generalized cutting criterion by numerical analysis.
2. For the steady-state chip formation in the micro-cutting process, the rake angle is usually constant, but the plowing angle is relative to the tool-edge precision and surface roughness on the workpiece.
3. While micro-specific coefficient \hat{K}_r is close to 1, the plowing zone will increase friction, stress, resistance, and even cutting excited-vibration or chipping, resulting in discontinuous chipping.
4. The variation of the rake angle will affect the cutting force and plowing zone according to Eq. (7). The average micro-cutting force $F_x = 0.5$ mN and $F_y = 0.22$ mN and micro-specific coefficient $\hat{K}_r = 0.44$; the maximum cutting temperature is distributed at 35–40°C.
5. Through fractal mathematics, the results presented optimal geometric parameters for micro-cutting simulation for tool HSS and workpiece_Al-7075: overlap ratio between cutters, average cut-depth ratio between cutters, and chip load (undeformed chip formation areas and shapes) distribution on cutter order.
6. The study proposed the mathematical model of micro-cutting resistance to predict the conditions at cutter-edge radius.

7. The average micro-cutting force $F_x = 0.5$ mN and $F_y = 0.22$ mN and specific coefficient $K_r = 0.44$; the maximum cutting temperature is distributed at 35–40°C. To compare the variation of rake angle, rake angle at 15° has smaller micro-cutting force, and hence, the tool design has longer tool life in the micro-cutting process.
8. The study developed the micro-MDOF cutting dynamics model and micro-fractal equation to simulate the micro-cutting process.
9. Due to suffering from the size effect of cutter-edge radius r in the micromachining process, the differential-cutter angle is relative to two factors: plowing angle and rake angle. For the steady-state chip formation in the micro-cutting process, the rake angle is usually constant, but the plowing angle is relative to the tool-edge precision and surface roughness on the workpiece.
10. From the view of the micro-cutting process, the definition of micro-specific coefficient is $\hat{K}_r = \frac{d\dot{x}}{df}$, and the definition of average micro-specific coefficient is $\hat{K}_{r, avg} = \frac{d\dot{x}_2 - d\dot{x}_1}{df_2 - df_1} = slope$.
11. To compare with micro-cutting, the traditional cutting process has the same plowing effect, but the plowing in microscope effect is more obvious as shown in **Figure 15**. The validation can be proven as the derived theory agreed with the simulation in the micro-cutting process.

Acknowledgements

This work was supported in part by Taiwan NSC under Grant No. MOST 105-2221-E-327-015 and the industrial plan—Development of Ultra Speed Intelligent CNC Band Saw Machine from No. 105RB07. Special thanks to Prof. Ching-Hua Wei, Prof. Chin-Tu Lu, Prof. Jung-Zen Huang, One-on-One group members and my good friend Sam Fang for supporting my study; Prof. Sheng-Jye Hwang, Prof. Ta-Hui Lin, and Prof. Rong-Shean Lee at NCKU for their support in the process of this study; and Prof. Yunn-Lin Hwang and Prof. Jeng-Haur Horng for their research cooperation at the National Formosa University.


Author details

Sung-Hua Wu

Department of Mechanical Engineering, National Cheng Kung University,
Tainan City, Taiwan (R.O.C)

*Address all correspondence to: jackywoo0923@gmail.com

IntechOpen

© 2019 The Author(s). Licensee IntechOpen. This chapter is distributed under the terms of the Creative Commons Attribution License (<http://creativecommons.org/licenses/by/3.0>), which permits unrestricted use, distribution, and reproduction in any medium, provided the original work is properly cited. 

References

- [1] Mandelbort BB. The Fractal Geometry of Nature. New York: W.H. Freeman; 1982
- [2] Cao ZY, He N, Li L. A finite element analysis of micro/meso-scale machining considering the cutting edge radius. *Applied Mechanics and Materials*. 2008; **10–12**:631-636. DOI: 10.4028/www.scientific.net/AMM.10-12.631
- [3] Wu S-H, Junz Wang J-J, Lee R-S. Chip fractal geometry and loading characteristics of sinusoidal multi-cutters in hack-sawing process. *International Journal of Machine Tools & Manufacture*. 2012;**59**:65-80. DOI: 10.1016/j.ijmachtools.2012.01.005
- [4] Wu S-H, Huang M-S, Jhou C-E, Wei C-C. Study on the cutting efficiency of high-speed band saw blade by Taylor tool life and fractal equations. In: *MATEC Web of Conferences*. Vol. 201. 2018. p. 01001. DOI: 10.105/mateconf/201820101001
- [5] Sung-Hua W. Optimal process parameters of shearing and plowing by fractal equation in micro-cutting strategy. In: *2016 International Conference on System Science and Engineering (ICSSE)*; Puli, Taiwan. DOI: 10.1109/ICSSE.2016.7551643
- [6] Adamsa DP, Vasileb MJ, Benavidesa G, Campbella AN. Micromilling of metal alloys with focused ion beam-fabricated tools. *Journal of the International Societies for Precision Engineering and Nanotechnology*. 2001;**25**:107-113
- [7] Dib MHM, Duduch JG, Jasinevicius RG. Minimum chip thickness determination by means of cutting force signal in micro end milling. *Precision Engineering*. January 2018;**51**:244-262. DOI: 10.1016/j.precisioneng.2017.08.016
- [8] Chae J, Park SS, Freiheit T. Investigation of micro-cutting operations. *International Journal of Machine Tools & Manufacture*. 2006; **46**:313-332. DOI: 10.1016/j.ijmachtools.2005.05.015
- [9] de Oliveira FB, Rodrigues AR, Coelho RT, de Souza AF. Size effect and minimum chip thickness in micromilling. *International Journal of Machine Tools & Manufacture*. 2015;**89**: 39-54. DOI: 10.1016/j.ijmachtools.2014.11.001
- [10] Zhang X, Ehmann KF, Yu T, Wang W. Cutting forces in micro-end-milling processes. *International Journal of Machine Tools & Manufacture*. 2016; **107**:21-40. DOI: 10.1016/j.ijmachtools.2016.04.012
- [11] Tansel IN, Arkan TT, Bao WY, Mahendrakar N, Shisler B, Smith D, et al. Tool wear estimation in micro-machining. Part I: Tool usage-cutting force relationship. *International Journal of Machine Tools & Manufacture*. 2000; **40**:599-608
- [12] Tansel IN, Arkan TT, Bao WY, Mahendrakar N, Shisler B, Smith D, et al. Tool wear estimation in micro-machining. Part II: Neural-network-based periodic inspector for nonmetals. *International Journal of Machine Tools & Manufacture*. 2000;**40**:609-620
- [13] Malekian M, Mostofa MG, Park SS, Jun MBG. Modeling of minimum uncut chip thickness in micro machining of aluminum. *Journal of Materials Processing Technology*. 2012;**212**: 553-559. DOI: 10.1016/j.jmatprotec.2011.05.022
- [14] Wu S-H, Lee R-S, Junz Wang J-J. Specific energy distributions for sinusoidal multi-cutters in groove-sawing process. *Journal of Materials Processing Technology*. 2013;**213**: 641-659. DOI: 10.1016/j.jmatprotec.2012.11.019

[15] Afazov SM, Zdebski D, Ratchev SM, Segal J, Liu S. Effects of micro-milling conditions on the cutting forces and process stability. *Journal of Materials Processing Technology*. 2013;**213**: 671-684. DOI: 10.1016/j.jmatprotec.2012.12.001

[16] Filiz S, Ozdoganlar B. A three-dimensional model for the dynamics of microendmills including bending, torsional and axial vibrations. *Precision Engineering*. 2011;**35**:24-37

[17] Filiz S, Conley C, Wasserman M, Ozdoganlar B. An experimental investigation of micro-machinability of copper 101 using tungsten carbide micro-endmills. *International Journal of Machine Tools and Manufacture*. 2007; **47**:1088-1100

[18] Afazov SM, Ratchev SM, Segal J, Popov AA. Chatter modelling in micro-milling by considering process nonlinearities. *International Journal of Machine Tools & Manufacture*. 2012;**56**: 28-38. DOI: 10.1016/j.ijmachtools.2011.12.010

[19] Afazov SM, Ratchev SM, Segal J. Prediction and experimental validation of micro-milling cutting forces of AISI H13 stainless steel at hardness between 35 and 60 HRC. *International Journal of Advanced Manufacturing Technology*. October 2012;**62**(9-12):887-899. DOI: 10.1007/s00170-011-3864-7

[20] Guo Q, Zhao B, Jiang Y, Zhao W. Cutting force modeling for non-uniform helix tools based on compensated chip thickness in five-axis flank milling process. *Precision Engineering*. 2018;**51**: 659-681. DOI: 10.1016/j.precisioneng.2017.11.009

[21] Malekian M, Park SS, Jun MBG. Modeling of dynamic micro-milling cutting forces. *International Journal of Machine Tools & Manufacture*. 2009; **49**:586-598. DOI: 10.1016/j.ijmachtools.2009.02.006